Talanta 107 (2013) 349–355

Contents lists available at SciVerse ScienceDirect

Talanta

journal homepage: www.elsevier.com/locate/talanta

Sodium dodecyl benzene sulfonate functionalized graphene for confined electrochemical growth of metal/oxide nanocomposites for sensing application

Shenghai Zhou [a], Donglei Wei [a], Hongyan Shi [a], Xun Feng [a], Kaiwen Xue [a], Feng Zhang [b], Wenbo Song [a,*]

[a] College of Chemistry, Jilin University, Changchun 130012, China
[b] State Key Laboratory of Inorganic Synthesis and Preparative Chemistry, Jilin University, Changchun 130012, PR China

ARTICLE INFO

Article history:
Received 29 September 2012
Received in revised form
11 January 2013
Accepted 17 January 2013
Available online 4 February 2013

Keywords:
Graphene
SDBS
Confined electrodeposition
Copper-based materials
Fructose

ABSTRACT

The electrochemical fructose sensor attracts considerable attention in the food industry and for clinical applications. Here, a novel fructose biosensor was developed based on immobilization of highly dispersed CuO–Cu nanocomposites on Graphene that was non-covalently functionalized by sodium dodecyl benzene sulfonate (SDBS) (denoted briefly as SDBS/GR/CuO–Cu). The structure and morphology of SDBS/GR/CuO–Cu were characterized by X-ray diffraction (XRD) and scanning electron microscopy (SEM). The electrochemistry and electrocatalysis were evaluated by cyclic voltammetry (CV). The fructose sensing performances were evaluated by chronoamperometry (i–t). Those properties were also compared with that of CuO–Cu. Results revealed the distinctly enhanced sensing properties of SDBS/GR/CuO–Cu towards fructose, showing significantly lowered overpotential of +0.40 V, ultrafast (< 1 s) and ultra-sensitive current response (932 μAm M^{-1} cm^{-2}) in a wide linear range of 3–1000 μM, with satisfactory reproducibility and stability. Those could be ascribed to the good electrical conductivity, large specific surface area, high dispersing ability and chemical stability of GR upon being functionalized non-covalently by SDBS, as well as the outstanding cation anchoring ability of SDBS on GR to resist aggregation among Cu-based nanoparticles during electro-reduction. More importantly, an improved selectivity in fructose detection was achieved. SDBS/GR/CuO–Cu is one of the promising electrode materials for electrochemical detection of fructose.

1. Introduction

Fructose, an insulin-independent monosaccharide, is relatively abundant in nature in fruits, vegetables, soft drinks and diabetic foods [1]. Its determination is extremely important for the food industry as well as in clinical and industrial applications. Several analytical methods like fluorometric [2], infrared spectroscopy [3], gas chromatography [4], and so forth have been applied to quantitatively monitor fructose in samples, and most of them are time-consuming and non-cost effective [5]. Simple and rapid detection methods are therefore required. The electrochemical determination method has recently attracted great attention because of its inherent advantages, including sensitivity, speed and miniaturization [6]. The well-known electrochemical biosensors for fructose determination are enzyme based, in which fructose dehydrogenase (FDH) is immobilized on a supporting electrode [7,8]. Fructose biosensing by FDH exhibits excellent selectivity and high sensitivity. However, like other enzyme based biosensors, the chief drawback is that the immobilized FDH easily lose their activity due to complex immobilization procedures and changeable microenvironment such as pH and temperature [9]. Therefore, detection of fructose using enzymeless sensors may be a more attractive strategy. We pioneered the fabrication of an enzyme-free fructose sensor in a previous report [10]. In this work, cobalt oxide-doped copper oxide composite nanofibers (CCNFs) were utilized as the active electrode material to construct a fructose sensor, which exhibited ultrafast and sensitive current response. Further exploring novel nanostructured electrode materials with high catalytic activity and good selectivity to realize direct and sensitive fructose determination still remains at the forefront of research.

Graphene (GR), an atomically thin 2D aromatic sheet composed of sp^2-bonded carbon atoms, is attracting considerable attention in the fields of batteries [11], super capacitors [12], sensors [13], transistors [14] and so forth [15]. Similar to carbon nanotubes (CNTs), the main challenge in the applications of graphene sheets is aggregation through strong π–π stacking and van der Waals interaction [16]. Dispersed graphene can be

* Corresponding author. Tel.: +86 431 85168352; fax: +86 431 85168420.
E-mail address: wbsong@jlu.edu.cn (W. Song).

0039-9140/$ - see front matter © 2013 Elsevier B.V. All rights reserved.
http://dx.doi.org/10.1016/j.talanta.2013.01.041

obtained by covalent and non-covalent functionalization approaches [17,18], in which non-covalent modification by DNA [19], and polymers [20], especially surfactants [21], often results in a stable dispersion of GR or CNT in water. And the damage to structure of the non-covalent modification route is negligible, which meets the challenge well. In this functionalization strategy, the surfactants assist the carbon materials dispersing well in aqueous media, because their charged groups (hydrophilic heads) attract to water and their alkyl chains (hydrophobic tails) adsorb on the surfaces of carbon materials [22]. Compared to other commonly employed surfactants such as sodium dodecyl sulfate (SDS), sodium dodecyl benzene sulfonate (SDBS) is an anionic surfactant that can enhance the stability of carbon materials in water [23,24]. The reason is that π-like stacking of the additional benzene rings in SDBS onto the surface of graphite increases the binding and surface coverage of surfactant molecules to graphite [23]. Zeng et al. recently fabricated stable dispersions of GR by heating the mixture of graphite oxide, hydrazine and SDBS, and no sediments were observed for at least two months [25]. Goak et al. and Wenseleers et al. demonstrated respectively that the intrinsic nature (purity and defect density) of CNT as well as amount of surfactants affected the dispersion of CNT in water [22,26]. Further work on developing stable GR dispersion by SDBS functionalization for catalysis and sensor application are still desirable.

Catalyst support plays an important role in the field of batteries [27], super-capacitors [28], direct alcohol fuel cells [29], electro-catalysis and sensing devices [30]. They are a class of materials utilized to load nano-sized functional materials, such as metals [31] and metal oxides [32], based on their unique properties such as high surface area, good mechanical resistance and chemical stability. Among support materials such as titanate [33], mesoporous silicates [34], metal–organic frameworks [35], and Graphene [36], Graphene possesses not only a large surface area and high chemical stability, but also good electrical conductivity. These unique properties render it a promising candidate for electrochemical sensor application. For example, metal/graphene (Au/GR) and metallic oxides/graphene (Co_3O_4/GR) exhibited excellent electrocatalytic activity toward O_2, H_2O_2, glucose and so forth [37,38]. In this study, a very stable GR dispersion was prepared by using the SDBS non-covalent modification strategy, and no sediments were observed for at least six months. The highly dispersed negative charges on SDBS/GR were further used to anchor functional metal cations on the basis of electrostatic self-assembled strategy. Upon electrochemical reduction, highly dispersed metal/oxide nanocatalysts with high electrochemical activity can be anticipated. Here, a SDBS/GR/CuO–Cu nanocomposite was prepared and attempted as the electrode material for fabrication of enzymeless fructose sensor.

2. Experiments

2.1. Reagents

GR was synthesized according to previously reported work [39]. D-Glucose, ascorbic acid (AA), oxalic acid (OA) and sodium dodecyl benzene sulfonate were obtained from Shanghai Co. Fructose, sucrose, maltose, and sodium hydroxide were purchased from Beijing Chemical Plant. Fructose injection was obtained from the first hospital of Jilin University. All chemicals were used as received without further purification. All solutions were prepared with ultrapure water. Fructose solutions were freshly prepared before each experiment.

2.2. Apparatus

The crystal structures of the samples were determined using an X-ray diffractometer (Siemens D5005, Munich, Germany). The morphologies of samples were viewed by SEM (SHIMADZU SSX-550, Japan). All electrochemical measurements were accomplished on a CHI 660A electrochemical workstation (CH instrument, USA). The SDBS/GR/CuO–Cu modified ITO electrode or CuO–Cu modified ITO electrode was used as the working electrode. A platinum wire electrode was applied as the counter electrode and a saturated calomel electrode (SCE) served as the reference electrode.

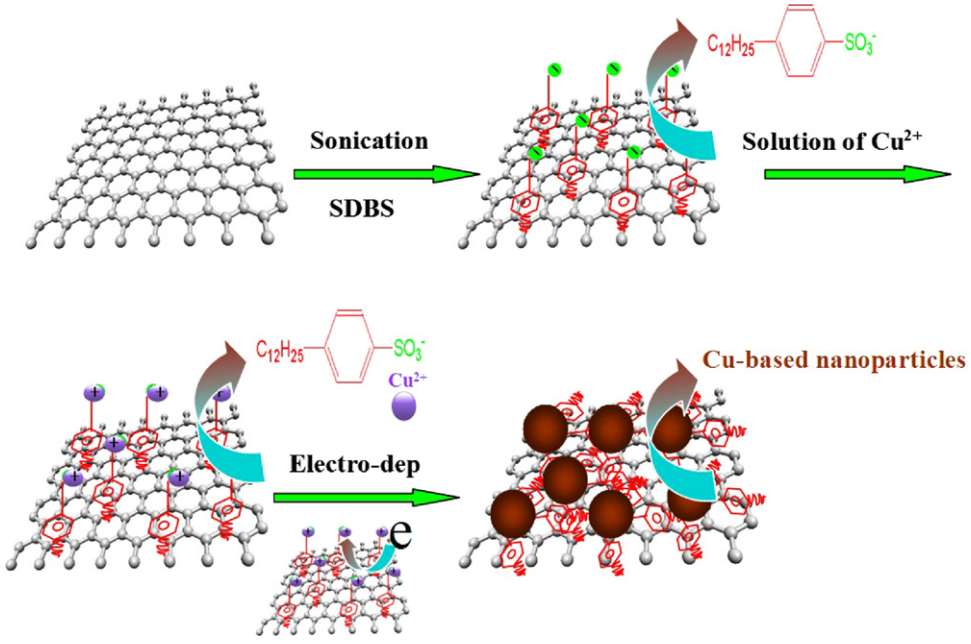

Fig. 1. Schematic representation of the preparation of the SDBS/GR/CuO–Cu nanocomposite film.

2.3. Preparation of SDBS/GR dispersion and SDBS/GR/CuO–Cu electrode

The SDBS/GR suspension was first prepared by dispersing 2 mg GR in 1 ml ultrapure water containing 10 mg SDBS, with sufficient ultrasonication for about 24 h. After storage for at least six months, the SDBS/GR dispersion was still very homogenous and stable, as shown in Fig. S1(a). In contrast, the GR dispersion (Fig. S1b) contains coagulated architectures at the bottom of vial. After dropping 5 μL of SDBS/GR suspension onto the cleaned ITO surface, the electrode was dried in air at laboratory temperature. Finally, the SDBS/GR/CuO–Cu nanocomposite electrode was prepared by the electrodeposited CuO–Cu nanocomposite onto the SDBS/GR/ITO slide in 0.05 M Na_2SO_4+0.05 M $CuSO_4$ solution at −0.9 V for 50 s. The preparation of the SDBS/GR/CuO–Cu nanocomposite is presented in Fig. 1. For comparison, the CuO–Cu nanocomposite electrodeposited onto an ITO surface without using the SDBS/GR support was also obtained similarly.

3. Results and discussion

3.1. Structure and morphology characterization of SDBS/GR/CuO–Cu nanocomposite

3.1.1. XRD diffraction analysis

To confirm the structure and composition of the samples, XRD analysis was carried out. The XRD patterns of the resultant products deposited on SDBS/GR/ITO (a) and ITO (b) substrates are presented in Fig. 2. All the diffraction peaks in each XRD pattern coincided well, indicating that the samples possess similar structure and composition under same deposition conditions. The peaks marked with an asterisk can be assigned to the Cu (PDF no. 89–2838, space group: Fm-3m), and the others marked with a circle ring are indexed to the CuO (PDF no.78–0428, space group: Fm-3m), suggesting a complex copper-based composite obtained by electrodeposition on the substrates.

3.1.2. SEM characterization

Fig. 3B shows the morphology of electrochemical-confined copper-based catalysts on SDBS/GR support characterized by SEM. The spherical shaped catalyst Cu-based nanodeposits dispersed uniformly and compactly on the surface of SDBS/GR with an average diameter of around 50 nm were achieved (Fig. 3B and its inset). While, as shown in Fig. 3A, the morphology of the Cu-based nanocomposites deposited on the ITO substrate without the SDBS/GR support was quite different. Large aggregations comprised of the branched Cu-based deposits with irregular structures were observed. The SDBS functionalized GR revealed quite flat sheets, as shown in Fig. 3C. The compact, uniform

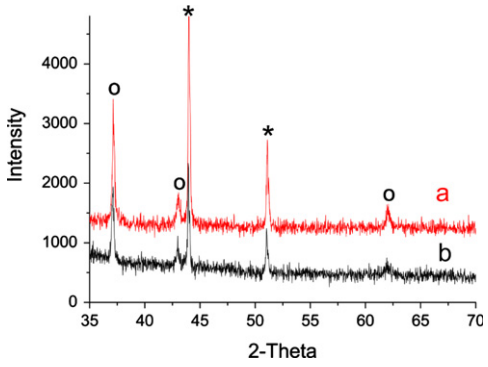

Fig. 2. XRD patterns of Cu-based materials on SDBS/GR/ITO (a) and ITO (b) substrates.

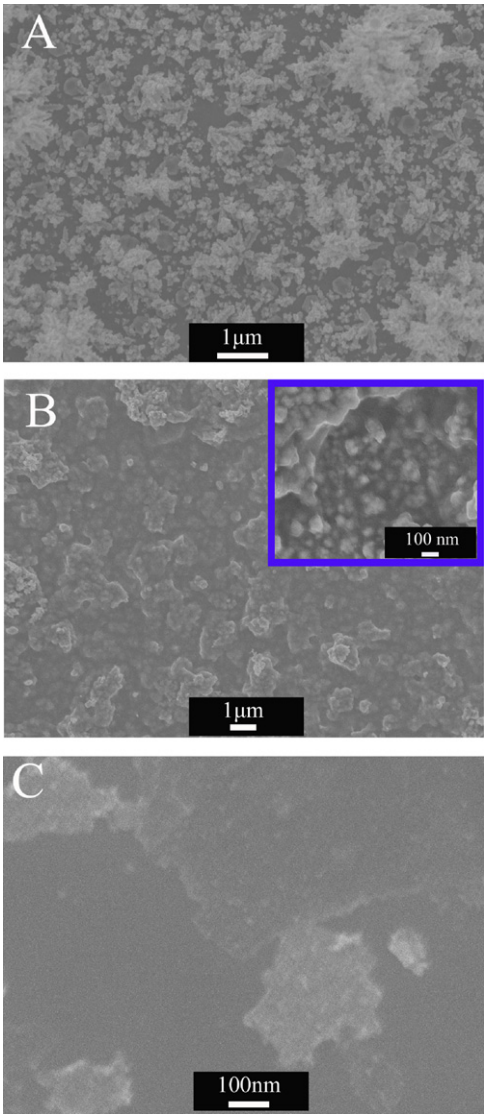

Fig. 3. SEM images of CuO–Cu nanocomposites on ITO (A) and SDBS/GR/ITO (B). SEM images of SDBS/GR (C).

particle size and the good dispersity of copper-based nanospheres on SDBS/GR were ascribed to the confined electrodeposition of Cu-based nanocomposites on the negatively charged SDBS anchoring layer supported by the GR sheet. It is well known that the microstructure and morphology of nanomaterials have a profound effect on its physical and chemical properties. In this work, the oxidation current of fructose at SDBS/GR/CuO–Cu/ITO was found to be much higher than that of CuO–Cu/ITO, suggesting an important role of the SDBS/GR support for loading highly dispersed and small-sized nanocatalysts.

3.2. Electrochemical characterization of SDBS/GR/CuO–Cu nanocomposites on ITO

3.2.1. Electrochemical activity of SDBS/GR/ITO

Cyclic voltammograms (CVs) of redox probes such as $Fe(CN)^{3-/4-}$, can provide important information for evaluating the electrochemical properties of the electrode materials. As shown in Fig. 4, the peak difference between anodic and cathodic peaks (ΔE_p) at the SDBS/GR/ITO electrode is 118 mV (curve a), which is 11 mV smaller than that of 129 mV at the bare ITO electrode (curve b). The smaller ΔE_p at the SDBS/GR/ITO

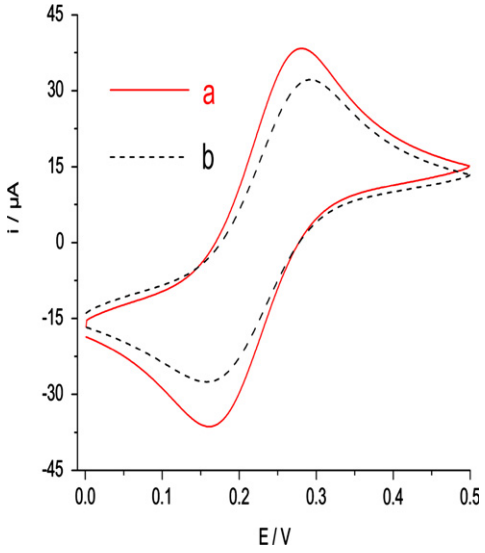

Fig. 4. Cyclic voltammograms obtained at SDBS/GR/ITO (a) and ITO (b) in 1 mM $Fe(CN)_6^{3-/4-}$/KCl solution.

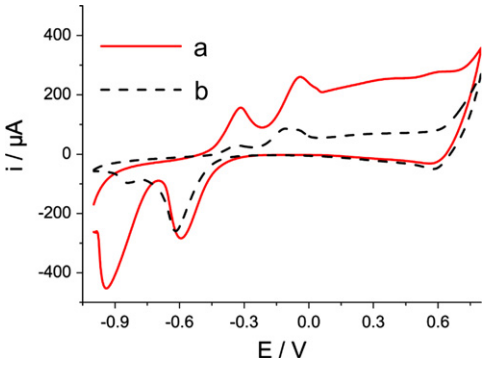

Fig. 5. Cyclic voltammograms of the electrodeposited copper on SDBS/GR (a) and ITO (b) in the potential range from −1.0 V to +0.8 V in 0.1 M NaOH.

electrode represents the higher electron transfer rate, due to the promotion of electron transfer rate by the presence of GR in the electrode configuration. Furthermore, compared with the bare ITO, the peak currents of the redox probe at SDBS/GR/ITO increased about 37%, and the electrochemical active area at SDBS/GR/ITO estimated from the charge during the redox processes increased up to 30%, with only 5 μl GR dispersion immobilized on the ITO surface. The above results suggest an improved electroactivity and facile charge transfer property of the SDBS/GR/ITO electrode.

3.2.2. *Electrochemical behaviors of SDBS/GR/CuO–Cu on ITO surface*

Facile charge transfer, improved electroactivity and highly negative charged sites of the SDBS/GR support provide an opportunity for electrochemically confining growth of metal-based nanocatalysts for sensing application. In this paper, electrodeposited CuO–Cu on the SDBS/GR support was obtained by the electrodeposition technique. For comparison, CuO–Cu electrodeposited onto an ITO surface without using the SDBS/GR support was also prepared under the same deposition conditions. In Fig. 5 (curve a), electrochemical characterization of the SDBS/GR/CuO–Cu nanocomposite was carried out by cyclic voltammetry in 0.1 M NaOH aqueous solution. Two anodic peaks, one at −0.32V and the other at −0.04V were observed during the oxidation process. The first peak is ascribed to the transition from Cu(0) to Cu(I), while the second peak is associated with the subsequent conversion of Cu(I) to Cu(II). Although no apparent wave emerged, it is generally believed that the formation of Cu(III) is at around +0.6 V, which could only be observed at a high concentration of NaOH [40]. On reversing the scan, the cathodic peak at about +0.58 V, corresponding to the reduction of Cu(III) to Cu(II), was observed, clearly indicating the presence of Cu(III). At about −0.6 V, Cu(II) was reduced to Cu(I), and the following rapid increase in the cathodic current at more negative potential was attributed to the reduction of Cu(I) to Cu(0). The electrochemical characteristics of SDBS/GR/CuO–Cu were similar to those of copper-titanate intercalation materials [41] and CuO nanoflowers [42] as well as other copper-based electrode materials in literature [43,44]. The presence of CuO–Cu nanocomposites on SDBS/GR revealed by electrochemical and XRD characterization demonstrated that the copper-based electrocatalyst was successfully loaded on the SDBS functionalized graphene support. For CuO–Cu electrodeposited similarly onto an ITO surface without SDBS/GR (curve b), very similar redox processes were found in the same potential range. However, the redox peak currents (at about −0.02 V) at SDBS/GR/CuO–Cu electrode were about 2.6 times as large as that at CuO–Cu/ITO electrode, implying a dramatically high electrochemical activity of the SDBS/GR/Cu electrode materials.

In order to investigate the electrochemical stability and oxidation activity of the SDBS/GR/CuO–Cu electrode, the potential range for voltammetric cycling was selected from 0 to 0.8 V. This potential range covers the oxidation transition from Cu(II) to Cu(III) redox couples, which is considered to play a key role in electro-oxidation of carbohydrate. The electrochemical data is recorded in Fig. 6(a). With the increase of scanning number, the oxidation current at SDBS/GR/CuO–Cu remains constant. Conversely, the oxidation current at CuO–Cu/ITO decreases gradually (Fig. 6b and inset). The above information suggested that SDBS/GR/CuO–Cu has better electrochemical stability compared to the contrastive CuO–Cu/ITO electrode. Furthermore, the oxidation current correlated with the formation of Cu(III) at +0.6 V at SDBS/GR/CuO–Cu is about 10 times as large as those of CuO–Cu/ITO, suggesting that the SDBS/GR/CuO–Cu nanocomposite possesses high electrochemical oxidation activity.

3.2.3. *Electro-oxidation of fructose at SDBS/GR/CuO–Cu electrode materials*

In this work, the electro-oxidation activity of SDBS/GR/CuO–Cu was evaluated by linear scanning voltammetry (LSV) in alkaline media by taking fructose as a probe, and compared with that of CuO–Cu/ITO. The LSV current responses at the above electrodes in the presence and absence of 0.2 mM fructose are presented in Fig. 7. Only a small background current was observed at the CuO–

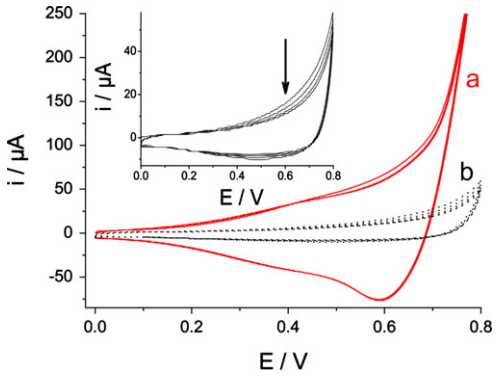

Fig. 6. Cyclic voltammograms of the electrodeposited CuO–Cu on SDBS/GR (a) and ITO (b) in the potential range from 0 V to +0.8V in 0.1 M NaOH. Inset: enlarged CVs at CuO–Cu/ITO.

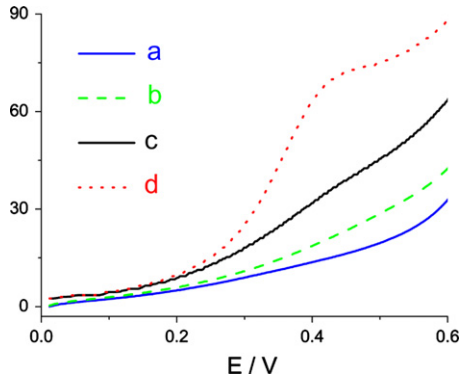

Fig. 7. Linear scanning voltammetry of CuO–Cu/ITO (a and b) and SDBS/GR/CuO–Cu/ITO (c and d) in 0.1 M NaOH in the absence (a and c) and presence (b and d) of 0.2 mM fructose, respectively.

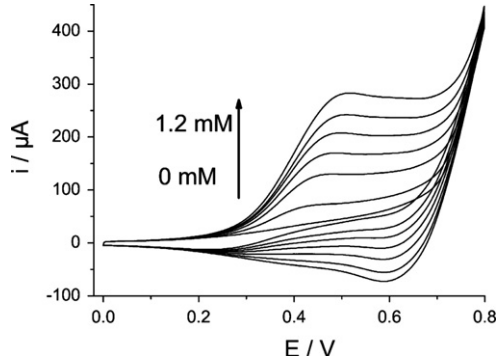

Fig. 8. CVs of SDBS/GR/CuO–Cu electrode recorded in 0.1 M NaOH in presence of 0 mM, 0.2 mM, 0.4 mM, 0.6 mM, 0.8 mM, 1.0 mM and 1.2 mM fructose, respectively.

Cu/ITO electrode in alkaline media (curve a), while a dramatic increase of current signal toward the positive end of the potential range was seen at SDBS/GR/CuO–Cu (curve c), which is ascribed to the role of GR in the increase of electroactivity at the composite electrode materials. In the presence of fructose, no obvious oxidation peak current is observed at the CuO–Cu/ITO electrode (curve b), suggesting the direct oxidation of fructose at the CuO–Cu/ITO electrode was not ideal. On the contrary, a significant increased oxidation peak of fructose at ca. +0.42 V (vs. SCE) was observed at SDBS/GR/CuO–Cu (curve d), indicating a high electro-oxidation ability of the SDBS/GR/CuO–Cu nanocomposite. The oxidative current of fructose at the SDBS/GR/CuO–Cu electrode was 6 times as large as that at the CuO–Cu/ITO electrode, which evidently demonstrated the advantages of SDBS functionalized GR support for CuO–Cu loading. These results indicate that the SDBS/GR/CuO–Cu nanocomposite is more active for fructose electro-oxidation than CuO–Cu, which only deposits on the ITO surface.

The concentration dependence of electrochemical activity of the SDBS/GR/CuO–Cu nanocomposite electrode toward oxidation of fructose was also studied. Fig. 8 shows the CVs of the SDBS/GR/CuO–Cu electrode recorded in 0.1 M NaOH in the absence and presence of 0.2 mM, 0.4 mM, 0.6 mM, 0.8 mM, 1.0 and 1.2 mM of fructose. The oxidation of fructose starts when the potential is more than 0.23 V, and an obvious oxidation peak is even observed at a low concentration of fructose such as 0.2 mM, suggesting a highly sensitive current response towards fructose oxidation. Interestingly, with the increase of fructose concentration, the oxidation peak potential was positively shifted from +0.42 V to +0.50 V. The reason is that the electron-transfer in the process of carbohydrate oxidation at the Cu-based nanoparticle surface was kinetically controlled [45]. As the fructose concentration increases, larger overpotential was needed to remove the adsorbed intermediates from the fructose oxidation, and the released active sites were available for further oxidation of fructose. With the increase of fructose concentration from low to high, another phenomenon seen is that the anodic peak current increases linearly, whereas the cathodic peak current decreases gradually, implying the possibility for quantitative determination of fructose using the as-prepared SDBS/GR/CuO–Cu electrode.

3.3. Amperometric performance of SDBS/GR/CuO–Cu in fructose determination

3.3.1. Optimum conditions

For a low detection limit and neglectable interference from other species, the choice of the detection potential is necessary for fructose detection. The amperometric current response of 0.15 mM fructose in a stirring electrolyte solution at the SDBS/GR/CuO–Cu nanocomposite electrode was measured at a constant interval of 0.05 V from +0.20 V to +0.65 V (Fig. 9). With the oxidation potential positively shifted, the oxidation current of fructose clearly increased. However, the S/B ratio initially kept on rising with potential, reached the topmost value at +0.40 V, and decayed while the potential positively shifted due to the increase in the baseline current at a higher potential. Thus, a constant potential of +0.40 V was selected and employed for all the subsequent amperometric detection.

3.3.2. Amperometric analysis

Amperometric analysis of fructose was carried out at the SDBS/GR/CuO–Cu nanocomposite electrode (Fig. 10, curve a) at +0.40 V by successive injection of fructose to 0.1 M NaOH. For comparison, the performance of the CuO–Cu/ITO electrode (Fig. 10, curve b) was also examined. From inset figures A and B, ultrafast current response (< 1 s) and good linearity toward fructose was observed at the SDBS/GR/CuO < Cu electrode in comparison with CuO < Cu/ITO. The linear range of fructose is from 3 to 1000 μM with the ultra-high sensitivity of 932 $\mu A m M^{-1} cm^{-2}$, and the linear regression equation is $I_{pa}=149.1C_{Fru}+0.16498$ ($R=0.994$).

In addition, the reproducibility and stability of the SDBS/GR/CuO–Cu nanocomposite electrode were also evaluated. The RSD of steady-state current response for five individually repetitive tests for 0.1 mM fructose was 3.5%, confirming a good reproducibility of the electrode. The current response decayed by 6.1% after six months storage, demonstrating a long-term storage stability of the electrode. The high stability and reproducibility of the SDBS/GR/CuO–Cu electrode in fructose determination may result from the high dispersity of SDBS/GR and Cu-based nanocatalysts that confined by the negatively charged SDBS.

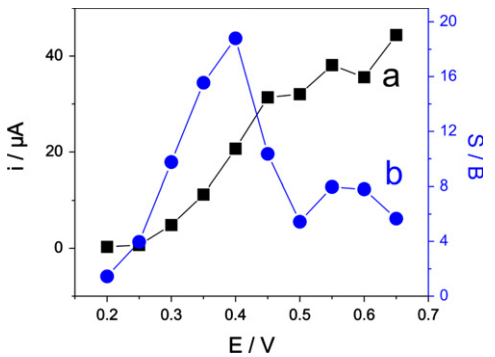

Fig. 9. Plots of oxidation current density (a) and signal-to-background ratio (b) to the applied potential at SDBS/GR/CuO–Cu film electrode obtained by chronoamperometry.

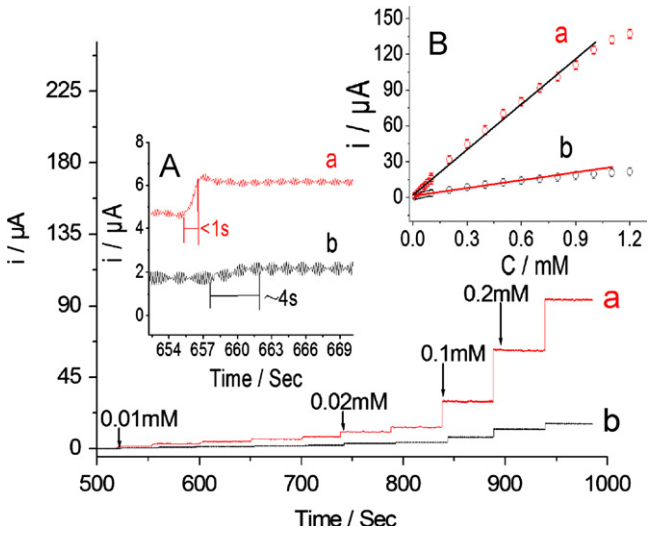

Fig. 10. Chronoamperometric responses of SDBS/GR/CuO–Cu (a) and CuO–Cu/ITO (b) in 0.1 M NaOH on injecting of fructose at +0.4 V. Inset A: enlarged chronoamperometric curves for clearly observing response time. Inset B: amperometric response to fructose concentration.

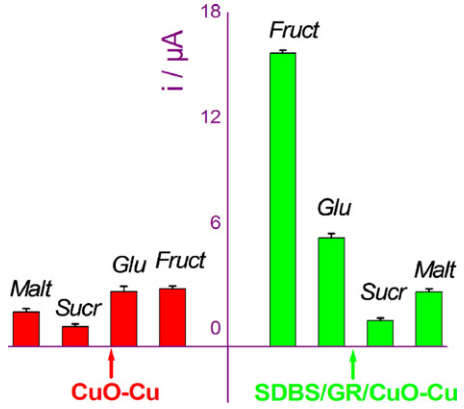

Fig. 11. Selectivity study for same concentration of fructose, glucose, sucrose and maltose at CuO–Cu/ITO and SDBS/GR/CuO–Cu electrodes, respectively.

3.3.3. Interferential analysis

Possible interfering species such as ascorbic acid (AA), oxalic acid (OA), ethanol and so forth were examined. Results in Table S1 revealed that ethanol, OA, and NaCl did not cause any observable interference to the designated concentration of fructose, whereas AA had a little interference effect to fructose. However, ascorbic acid is only 2–3% of the concentration of fructose in samples such as citrus juice [46]. Consequently, its interference can be ignored in the analysis of these samples.

The response of the developed fructose sensor to other sugars (e.g. glucose, sucrose and maltose) was also investigated. In this study, the concentrations of all sugars including fructose were all 0.1 mM. As shown in Fig. 11, the SDBS/GR/CuO–Cu nanocomposite electrode indeed promotes the oxidation of all sugars to a higher extent compared to the CuO–Cu/ITO electrode, attributed to the improved electroactivity of the SDBS/GR/CuO–Cu by Cu-based catalyst confining on SDBS/GR support. More importantly, one can obviously see from the data that the ratio of glucose oxidation current to fructose oxidation current decreases from 93% at CuO–Cu/ITO electrode to 33% at the SDBS/GR/CuO–Cu electrode, suggesting the dramatically improved selectivity at SDBS/GR/CuO–Cu electrode materials. The main reason for the specificity of SDBS/GR/CuO–Cu may be ascribed to (a) GR or (b) SDBS. However, by referring related literature [47–49], the metal/graphene (Cu/GR and PtNi/GR), metal oxides/graphene (Co_3O_4/GR and CuO/GR) and metal hydroxides/graphene ($Ni(OH)_2$/GR) nanocomposites all exhibited good specificity for glucose oxidation. GR seems not the key component serving for fructose selectivity in the SDBS/GR/CuO–Cu electrode. And the main reason for the SDBS/GR/CuO–Cu electrode differing from CuO–Cu may be related with SDBS. Along this line of thought, additional experiment was carried out by fabricating SDBS onto the CuO–Cu nanocomposite and measuring the respective electro-oxidation current of fructose and glucose. From Fig. S2, one can see that fructose oxidation current is about 2.4 times of glucose, indicating the specificity of SDBS functionalized electrode towards fructose. This selectivity may relate with the unique molecular structure of SDBS and its functional groups, which may provide favorable microenvironment to interact with the D-fructose molecule.

Table 1
Comparison of the performances of SDBS/GR/CuO–Cu electrode with some other relevant ones.

Electrode configuration	Type	Sensitivity ($\mu A m M^{-1} cm^{-2}$)	Linear range	Response time (s)	Reference
FDH–Pt	Enzyme	8.78	3–13 mM	ca 25	[46]
FDH–CNT	Enzyme	3.04	5 μM–2 mM	–	[50]
FDH–Au	Enzyme	19.17	2–100 μM	–	[51]
FDH–Fc–CA	Enzyme	0.82	–	45	[52]
CuO/Co_3O_4 NFs	Non-enzyme	268.7	10 μM–6 mM	1	[10]
SDBS/GR/CuO–Cu	Non-enzyme	931.8	3–1000 μM	<1	This work

A comparison of the performances of the SDBS/GR/CuO–Cu electrode with some other relevant sensors is presented in Table 1. It can be seen that the proposed sensor exhibits superior characteristics in terms of ultrahigh sensitivity, ultrafast response and wide linear range.

3.3.4. Real sample analysis

In order to evaluate the applicability of the prepared sensor, fructose injections used usually by diabetic and chronic liver disease patients were selected as real samples for analysis. Prior to measurements, the sample was diluted to 100 times with water without any treatment. And the determinations were performed at +0.4 V in 5 ml 0.1 M NaOH and the results are listed in Table S2. The values determined were satisfactory with a good recovery. Furthermore, the results of this biosensor also agreed well with the data obtained by the Fructose assay kit, a well-established method for fructose determination, indicating the accuracy of this method.

4. Conclusion

A Graphene aqueous solution with good dispersion (no sediments observed for at least six months) was obtained based on a non-covalent modification strategy by attracting the charged groups of SDBS to water and adsorbing the alkyl chains on the surface of GR. Highly negative charged site, facile charge transfer ability and large surface area of the SDBS/GR support are expected to provide an opportunity for electrochemically confined growth of nanosized metal/oxide catalysis for sensing application. Highly compact and uniformly dispersed CuO–Cu nanocomposites were electrogenerated on SDBS/GR in this study; its electrochemical activity for fructose oxidation was greatly enhanced in comparison with that of CuO–Cu/ITO. Assay performances towards fructose at SDBS/GR/CuO–Cu were significantly improved with low detection potential, ultrafast and sensitive current response,

as well as improved selectivity, implying one of the promising electrode materials in sensor fabrication.

Acknowledgments

This work was supported by the National Natural Science Foundation of China under Grants 21075048 and 20543003, as well as the Scientific Research Foundation for Returned Overseas Chinese Scholars, State Education Ministry of China.

Appendix A. Supporting information

Supplementary data associated with this article can be found in the online version at http://dx.doi.org/10.1016/j.talanta.2013.01.041.

References

[1] P.A. Paredes, J. Parellada, V.M. Fernández, I. Katakis, E. Domínguez, Biosens. Bioelectron. 12 (1997) 1233–1243.
[2] W. Tan, D. Zhang, Z. Wang, C. Liu, J. Mater. Chem. 17 (2007) 1964–1968.
[3] M. Cascant, J. Kuligowski, S. Garrigues, M.D.L. Guardia, Talanta 85 (2011) 1721–1729.
[4] P.N. Wahjudi, M.E. Patterson, S. Lim, J.K. Yee, C.S. Mao, W.-N.P. Lee, Clin. Biochem. 43 (2010) 198–207.
[5] J. Biscay, E.C. Rama, M.B.G. García, A.J. Reviejo, J.M.P. Carrazón, A.C. García, Talanta 88 (2012) 432–438.
[6] S. Tsujimura, A. Nishina, Y. Kamitaka, K. Kano, Anal. Chem. 81 (2009) 9383–9387.
[7] U.B. Trivedi, D. Lakshminarayana, I.L. Kothari, P.B. Patel, C.J. Panchal, Sens. Actuators B 136 (2009) 45–51.
[8] M. Tominaga, S. Nomura, I. Taniguchi, Biosens. Bioelectron. 24 (2009) 1184–1188.
[9] P. Holt-Hindle, S. Nigro, M. Asmussen, A.C. Chen, Electrochem. Commun. 10 (2008) 1438–1441.
[10] Y. Wang, W. Wang, W.B. Song, Electrochim. Acta 56 (2011) 10191–10196.
[11] L.M. Dai, D.W. Chang, J.B. Baek, W. Lu, Small 8 (2012) 1130–1166.
[12] X. Huang, X.Y. Qi, F. Boey, H. Zhang, Chem. Soc. Rev. 41 (2012) 666–686.
[13] Y.X. Liu, X.C. Dong, P. Chen, Chem. Soc. Rev. 41 (2012) 2283–2307.
[14] F. Schwierz, Nat. Nanotech. 5 (2010) 487–496.
[15] T. Kuila, S. Bose, A.K. Mishra, P. Khanr, N.H. Kim, J.H. Lee, Prog. Mater. Sci. 57 (2012) 1061–1105.
[16] D. Li, M.B. Muller, S. Gilje, R.B. Kaner, G.G. Wallance, Nat. Nanotechnol. 3 (2008) 101–105.
[17] T. Kuila, S. Bose, A.K. Mishra, P. Khanra, N.H. Kim, J.H. Lee, Prog. Mater. Sci. 57 (2012) 1061–1105.
[18] V. Georgakilas, M. Otyepka, A.B. Bourlinos, V. Chandra, N. Kim, K.C. Kemp, P. Hobza, R. Zboril, K.S. Kim, Chem. Rev. 112 (2012) 6156–6214.
[19] J. Liu, Y. Li, Y. Li, J. Li, Z. Deng, J. Mater. Chem. 20 (2010) 900–906.
[20] J. Liu, W. Yang, L. Tao, D. Li, C. Boyer, T.P. Davis, J. Polym. Sci. Pol. Chem. 48 (2010) 425–433.
[21] K. Zhang, L. Mao, L.L. Zhang, H.S.O. Chan, X.S. Zhao, J.S. Wu, J. Mater. Chem. 21 (2011) 7302–7307.
[22] J.C. Goak, S.H. Lee, J.H. Han, S.H. Jang, K.B. Kim, Y. Seo, Y.S. Seo, N. Lee, Carbon 49 (2011) 4301–4313.
[23] M.F. Islam, E. Rojas, D.M. Bergey, A.T. Johnson, A.G. Yodh, Nano Lett. 3 (2003) 269–273.
[24] M. Bystrzejewski, A. Huczko, H. Lange, T. Gemming, B. Büchner, M.H. Rümmeli, J. Colloid Interf. Sci. 345 (2010) 138–142.
[25] Q. Zeng, J.S. Cheng, L.H. Tang, X.F. Liu, Y.Z. Liu, J.H. Li, J.H. Jiang, Adv. Funct. Mater. 20 (2010) 3366–3372.
[26] W. Wenseleers, I.I. Vlasov, E. Goovaerts, E.D. Obraztsova, A.S. Lobach, A. Bouwen, Adv. Funct. Mater. 14 (2004) 1105–1112.
[27] Y.Q. Zhang, X.H. Xia, X.L. Wang, Y.J. Mai, S.J. Shi, Y.Y. Tang, C.G. Gu, J.P. Tu, J. Power Sources 213 (2012) 106–111.
[28] H. Jiang, J. Ma, C.Z. Li, Adv. Mater. 24 (2012) 4197–4202.
[29] N.G. Shang, P. Papakonstantinou, P. Wang, S.R.P. Silva, J. Phys. Chem. C 114 (2012) 15837–15841.
[30] Y.Y. Liang, H.L. Wang, J.G. Zhou, Y.G. Li, J. Wang, T. Regier, H.J. Dai, J. Am. Chem. Soc. 134 (2012) 3517–3523.
[31] X. Yang, Q.D. Yang, J. Xua, C.S. Lee, J. Mater. Chem. 22 (2012) 8057–8062.
[32] F. Xiao, Y.Q. Li, X.L. Zan, K. Liao, R. Xu, H.W. Duan, Adv. Funct. Mater. 22 (2012) 2487–2494.
[33] S.F. Tong, Y.H. Xue, Z.X. Zhang, W.B. Song, J. Phys. Chem. C 114 (2010) 20925–20931.
[34] J. Zhi, D.P. Song, Z.W. Li, X. Lei, A.G. Hu, Chem. Commun. 47 (2011) 10707–10709.
[35] L.B. Vilhelmsen, K.S. Walton, D.S. Sholl, J. Am. Chem. Soc. 134 (2012) 12807–12816.
[36] H.C. Gao, F. Xiao, C.B. Ching, H.W. Duan, Appl. Mater. Interfaces 3 (2011) 3049–3057. (3).
[37] J.G. Hua, F.H. Li, K.K. Wang, D.X. Han, Q.X. Zhang, J.H. Yuan, L. Niu, Talanta 93 (2012) 345–349.
[38] X.W. Wang, X.C. Dong, Y.Q. Wen, C.M. Li, Q.H. Xiong, P. Chen, Chem. Commun. 48 (2012) 6490–6492.
[39] C.S. Shan, H.F. Yang, J.F. Song, D.X. Han, A. Ivaska, L. Niu, Anal. Chem. 81 (2009) 2378–2382.
[40] P.F. Luo, S.V. Prabhu, R.P. Baldwin, Anal. Chem. 62 (1990) 752–755.
[41] S.F. Tong, H.Y. Jin, D.F. Zheng, W. Wang, X. Li, Y.H. Xue, W.B. Song, Biosens. Bioelectron. 24 (2009) 2404–2409.
[42] M.J. Song, S.W. Hwang, D. Whang, Talanta 80 (2010) 1648–1652.
[43] Y.C. Zhang, L. Su, D. Manuzzi, H. Monteros, W.Z. Jia, D.Q. Huo, C.J. Hou, Y. Lei, Biosens. Bioelectron. 31 (2012) 426–432.
[44] H.B. Hassanl, Z.A. Hamid, Int. J. Electrochem. Sci. 6 (2011) 5741–5758.
[45] S.R. Crouch, T.F. Cullen, Anal. Chem. 70 (1998) 53–106.
[46] U.B. Trivedi, D. Lakshminarayana, I.L. Kothari, P.B. Patel, C.J. Panchal, Sens. Actuators B Chem. 136 (2009) 45–51.
[47] J. Luo, H.Y. Zhang, S.S. Jiang, J.Q. Jiang, X.Y. Liu, Microchim. Acta 177 (2012) 485–490.
[48] L.Q. Luo, L.M. Zhu, Z.X. Wang, Bioelectrochemistry 88 (2012) 156–163.
[49] N.Q. Qiao, J.B. Zheng, Microchim. Acta 177 (2012) 103–109.
[50] R. Antiochia, I. Lavagnini, F. Magno, Anal. Lett. 37 (2004) 1657–1669.
[51] S. Campuzano, V. Esamilla-Gómez, M.Á. Herranz, M. Pedrero, J. Pingrrón, Sens. Actuators B Chem. 134 (2008) 974–980.
[52] J. Tkáč, I. Voštiar, E. Šturdík, P. Gemeiner, V. Mastihuba, J. Annus, Anal. Chim. Acta 439 (2001) 39–46.